# Soft Matter



View Article Online **PAPER** 



Cite this: Soft Matter, 2022, **18**, 3793

Received 27th January 2022, Accepted 21st April 2022

DOI: 10.1039/d2sm00130f

rsc.li/soft-matter-journal

# Crosslinking and depletion determine spatial instabilities in cytoskeletal active matter†

Guillaume Sarfati, Ananyo Maitra, b Raphael Voituriez, ac Jean-Christophe Galas \*\* and André Estevez-Torres \*\*

Active gels made of cytoskeletal proteins are valuable materials with attractive non-equilibrium properties such as spatial self-organization and self-propulsion. At least four typical routes to spatial patterning have been reported to date in different types of cytoskeletal active gels: bending and buckling instabilities in extensile systems, and global and local contraction instabilities in contractile gels. Here we report the observation of these four instabilities in a single type of active gel and we show that they are controlled by two parameters: the concentrations of ATP and depletion agent. We demonstrate that as the ATP concentration decreases, the concentration of passive motors increases until the gel undergoes a gelation transition. At this point, buckling is selected against bending, while global contraction is favored over local ones. Our observations are coherent with a hydrodynamic model of a viscoelastic active gel where the filaments are crosslinked with a characteristic time that diverges as the ATP concentration decreases. Our work thus provides a unified view of spatial instabilities in cytoskeletal active matter

#### 1 Introduction

Active matter is composed of agents that transform free energy into mechanical work, thus making non-equilibrium materials with attractive properties such as spatial self-organization and self-propulsion. 1-3 In this context, cytoskeletal active matter, constituted of protein filaments set in motion by molecular motors, is particularly interesting because the collective interaction of nanometric subunits creates order at the macroscopic scale. However, the determinants of spatial self-organization in these active systems are not yet well understood. 3-Dimensional cytoskeletal active matter is prone to at least four different spatial instabilities: (i) bending,4 (ii) buckling,5-7 (iii) global8-11

Here we consider a mixture composed of microtubules (MTs), kinesin motor clusters that pull on them and a depletant that generates microtubule bundles. 13 In the presence of ATP, this mixture generates an active solution in 3-dimensions that we will call 'Dogic system' in the following. When the MTs are stabilized with GMPCPP they are shorter and the Dogic system generates continuous chaotic flows13 through an in-plane bending instability both in 2D<sup>14</sup> and in 3D.<sup>4</sup> When the MTs are stabilized with taxol they are longer and chaotic flows are still observed but they emerge only after an out-of-plane buckling instability that creates a corrugated sheet.<sup>5,6</sup> Bending<sup>15</sup> and buckling<sup>7</sup> have also been reported in actin-myosin gels.

Besides bending and buckling instabilities, global and local contractions have been reported both in actin-myosin gels<sup>8,10</sup> and in MT-motors mixtures. 9,11,12,16 In the Dogic system, global contractions appear with taxol MTs,6,17-19 while local contractions arise with GMPCPP MTs. 18,19 Very recent experiments, however, have observed both types of contractions with GMPCPP MTs.<sup>20</sup> Finally, dynamic microtubules in the presence of multiheaded-kinesins yield chaotic flows or local contractions in the absence of depletant<sup>21</sup> depending on the ratio

and (iv) local contractions. 9,10,12 These instabilities have been observed experimentally but so far in different systems, thus precluding a unified analysis of potential transitions between all possible phases. Further, there is currently no clear theoretical understanding of how a gel transitions from one instability mode to another.

<sup>&</sup>lt;sup>a</sup> Sorbonne Université, CNRS, Institut de Biologie Paris-Seine (IBPS), Laboratoire Jean Perrin, (LJP), F-75005 Paris, France. E-mail: jean-christophe.galas@sorbonne-universite.fr, andre.estevez-torres@sorbonne-universite.fr

b Laboratoire de Physique Théorique et Modélisation, CNRS UMR 8089, CY Cergy Paris, Université, F-95302 Cergy-Pontoise Cedex, France

<sup>&</sup>lt;sup>c</sup> Sorbonne Université, CNRS, Laboratoire de Physique Théorique de la Matière Condensée, (LPTMC), F-75005 Paris, France

<sup>†</sup> Electronic supplementary information (ESI) available: Experimental and theory details, including Fig. S1-S8 and Tables S1-S4. Movie S1, S2: Time-lapse microscopy of microtubules displaying a bending instability. Movie S3, S4: Time-lapse microscopy of microtubules displaying a buckling instability. Movie S5, S6: Timelapse epifluorescence microscopy of microtubules displaying local (S5) and global (S6) contractions. Movie S7, S8: Time-lapse epifluorescence microscopy of microtubules displaying different instabilities depending on the concentration of passive linkers at constant [ATP] and pluronic. See DOI: https://doi.org/10.1039/

between MT growth and motor speed, and the ratio between the motor and MT concentration. In summary, the disparity of conditions in which spatial instabilities have been observed in cytoskeletal active matter (Table S2, ESI†) hinders our understanding of these systems. Here, we demonstrate that the four instabilities can be observed in the Dogic system by tuning only two parameters: ATP and depletant concentrations. The transition from bending to buckling and from local to global contractions happens at a critical ATP concentration that is associated to a critical concentration of passive motors that induces a gelation transition between a liquid-like and a solid-like state.<sup>22</sup> A similar transition is observed at constant ATP concentration when the concentration of a passive linker is increased, which supports its generic physical origin, independently of the specific nature of the crosslinking agents.

#### 2 Results and discussion

Our experiments take place in a long and thin channel of rectangular cross-section with typical dimensions  $L \times W \times H = 10 \times 1 \times 0.1 \text{ mm}^3$ . The active solution is composed of short GMPCPP-stabilized microtubules, clusters of biotinylated kinesin-1 in the presence of streptavidin, the depletant agent pluronic, that forms MTs bundles, and ATP coupled to an

ATP-regeneration system (see Fig. 1a and Methods, ESI†). MTs are fluorescent and they are imaged using either confocal or epifluorescence microscopy. When the solution is pipetted into the channel, the shear flow generates an initial nematic order along the *x*-axis.

At high pluronic concentration (5.5% w/v), the nematic state is deformed in two different ways depending on the ATP concentration, before chaotic flow occurs. At 50 uM ATP, the MT bundles deform in the xy-plane forming waves with a typical wavelength of 250 µm along the x-axis that arises within 5 minutes (Fig. 1b, c and Movie S1, ESI†). Confocal images show a minimal deformation of the bundles in the xz-plane. This in-plane bending instability has recently been observed in a similar system both in 3D4 and in 2D.14 Within 10-20 min, a superposition of bending instabilities results in a chaotic flow of bundles (Movie S2, ESI†). At 5 μM ATP, in contrast, the MTs deform in the xz-plane, creating an undulating sheet with a typical wavelength of 200 µm within 150 min (Fig. 1d, e and Movie S3, ESI†). Buckling happens concomitantly with a 10% compression of the height of the gel. In the xy-plane, this sheet appears as a periodic structure of black and bright zones, with preserved nematic order of MT bundles along the x-axis. Within 1500 min this instability conduces to an onset of chaotic flows destroying nematic order, although the slow dynamics preclude the observation of a fully developed chaotic state (Movie S4, ESI†).

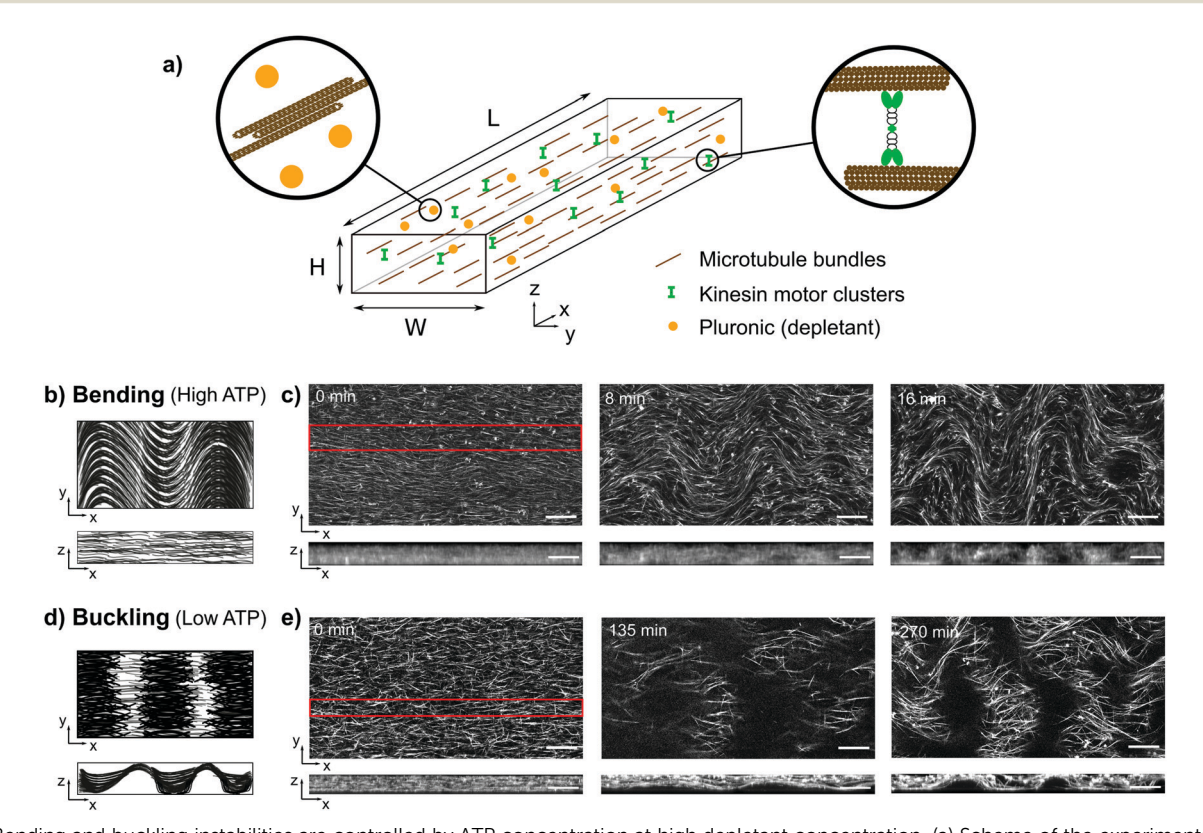


Fig. 1 Bending and buckling instabilities are controlled by ATP concentration at high depletant concentration. (a) Scheme of the experimental system with the microtubules in brown, the motor clusters in green and the pluronic depletant in orange, inside a rectangular channel. Cartoons of the microtubule morphology during the bending (b) and buckling (d) instabilities (the MTs appear in black). Time-lapse confocal images of fluorescent microtubules showing the bending (c) and buckling (e) from the bottom (xy-plane) and from the side (xz-plane) of the channel (the MTs appear in white). 5.5% pluronic, [ATP] = 50  $\mu$ M for bending and 5  $\mu$ M for buckling. Scale bars are 200  $\mu$ m.

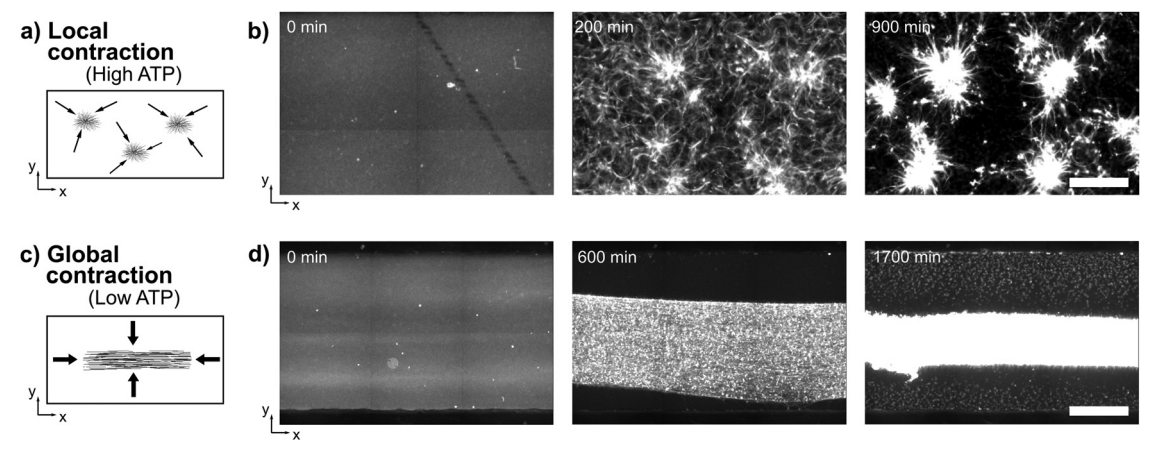


Fig. 2 Global and local contractions are controlled by ATP concentration at low depletant concentration. Cartoons of the microtubule morphology during local (a) and global (c) contractions (the MTs appear in black). Time-lapse epifluorescence images for local (b) and global contractions (d) in the yx-plane (the MTs appear in white). 1.5% pluronic, [ATP] =  $5 \mu M$  for global and 100  $\mu M$  for local contractions. Scale bars are 500  $\mu M$ .

This out-of-plane buckling instability has recently been reported in a system that is similar but displays two important differences: longer, taxol-stabilized MTs, and much higher [ATP] (2 mM).<sup>5,6</sup> Note however that, to the best our knowledge, the bending to buckling transition has not been observed so far.

At a lower pluronic concentration (1.5%) the behavior of the system changes dramatically (Fig. 2). In these conditions and high [ATP] (100 μM), a chaotic flow is observed during the first 100 min but afterwards microtubules aggregate, their area growing with an exponential rate of 0.028 min<sup>-1</sup>, first to make 20 µm diameter clumps that coalesce after 1500 min into  $\sim 250 \, \mu \text{m}$  diameter aggregates separated by a typical distance of  $\sim 500 \, \mu m$  (Movie S5, ESI†). We call this late instability local contractions. At the time resolution of the experiments, the type of instability that yields the initial chaotic flow could not be resolved. In contrast, at low [ATP] (5 μM), a global contraction in the absence of chaotic flow is observed (Movie S6, ESI†). The MT network first contracts along y with an onset rate of  $0.015 \text{ min}^{-1}$  until it reaches a steady-state width of 0.3W at t = 1000 min and later contracts along x until contraction stops at 1700 min. This transition from local to global contraction reminds the one reported for actomyosin gels, where a critical concentration of passive linkers induced the percolation of the gel yielding the global contraction state.<sup>10</sup>

Fig. 3 recapitulates the phase diagram of spatial instabilities as a function of depletant and ATP concentrations. The transition between bending and buckling happens at a critical concentration [ATP]<sub>c</sub> in the range 5–10 μM. When the pluronic concentration increases, the [ATP]<sub>c</sub> marginally increases. Note that the characteristic time of the instability strongly decreases with increasing [ATP] (Fig. S2 and Table S3, ESI†), with buckling being significantly slower than bending, except at [ATP]<sub>c</sub> where replicate experiments yield either one or the other instability or a mixture of the two (Fig. S3, ESI†), with identical time-scales.

The transition between local and global contractions also happens at  $[ATP]_c = 10 \mu M$ , suggesting that ATP plays a similar role in both processes. Interestingly, for long, taxol-stabilized

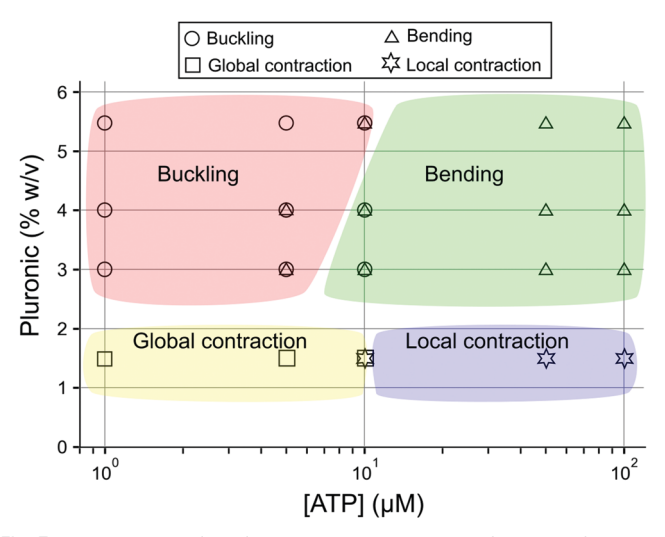


Fig. 3 Phase space of the four spatial instabilities as a function of pluronic and ATP concentrations. The symbols indicate the observed instabilities in a triplicate experiment and the colors are a guide to the eye.

MTs a similar phase diagram was observed, although with some differences (Fig. S4, ESI†). First, the bending/buckling and local/global transition happened at a slightly higher ATP concentration. Second, the limit between contracting and extensile instabilities occurred at a lower depletant concentration. Finally, in some occasions, buckling and bending ended up producing, respectively, global and local contractions instead of chaotic flows. We hypothesize that these differences mainly result from the increased length of taxol-stabilized MTs, which would favor gelation at a lower concentration of passive crosslinkers (and thus higher [ATP]) and the formation of bundles at a lower depletant concentration.

In a recent and complementary work, Lemma et al. established the phase diagram of a similar active gel as a function of tubulin, depletant and motor concentration at high ATP concentration.20 They observed the following phases: global

and local contractions, active foams, and bending, but not buckling. In particular, Lemma et al. found that increasing depletant promoted the transition from local to global contractions and from these to bending. In our case, depletant concentration induced a transition from global contractions to buckling and from local contractions to bending.

In the following, we will elucidate the effect of [ATP] on the spatial instabilities of the gel by considering two alternative hypothesis. In the kinetic hypothesis, the bending/buckling transition happens when there is a cross-over in the characteristic times of two concurrent processes: the passive contraction of the gel in the z direction promoting buckling, and the activity of the motors, favoring bending, that increases with [ATP]. In the gelation hypothesis, instead, [ATP] influences the concentration of inactive motors that act as passive crosslinkers of the gel inducing a gelation transition below a critical ATP concentration. We demonstrate that the gelation hypothesis is the only coherent with our experimental observations.

#### 2.1 The bending/buckling transition is not controlled by passive contraction

Senoussi et al. and Strübing et al. observed a buckling instability at high [ATP] in the presence of long MTs. 5,6 In ref. 5, the MTs contracted along z due to passive depletion forces to form a film that buckled because of the negative surface tension induced by the motors. Our first hypothesis is thus that the reduction in [ATP] reduces the activity and lets the time for the passive contraction to form a film that buckles. In this kinetic hypothesis two processes are in competition: the passive contraction of MTs into a film, whose time-scale would be independent of [ATP], and the activity due to the motors, whose dynamics may depend on [ATP] (Fig. 4a). To test it we first measured the passive contraction

dynamics along z in the absence of ATP (Fig. S5, ESI†). In the absence of pluronic but in the presence of motors a slight 5% expansion of the gel was observed. The strongest contraction, 50% of the thickness of the gel, was observed in the presence of pluronic alone and it reached 30% when both kinesin and pluronic were present. The characteristic time of passive contraction in these two cases was in the range 150-200 min (Fig. S5, ESI†).

We then repeated the bending/buckling experiment in Fig. 1 but using caged-ATP to let the passive contraction happen in the absence of activity. Initially, the two systems at 5 and 50 μM caged-ATP evolved in the absence of free ATP and after 4 h a light pulse uncaged it (Fig. 4). In both cases, MTs contracted slightly along z during the first 4 h (Fig. S5b, ESI $\dagger$ ). After uncaging, buckling with preserved nematic order along x was observed at 5 μM ATP within 15 min (Fig. 4b and d). At 50 μM ATP, uncaging resulted in a bending instability destroying nematic order along x (Fig. 4c and e), as in happened in Fig. 1c, although the bending was less clear. Indeed, this is expected because, as discussed in the following, a suspended film that bends in the xy-plane necessarily deforms in the xz-plane. Importantly, however, pure buckling was not observed at 50 µM ATP even though the uncaging occurred after the MTs film was formed. This result thus invalidates the kinetic hypothesis.

#### 2.2 A passive crosslinker-based theory to explain the transition from one instability mode to another

Gagnon et al. used micro-rheology experiments to show that reducing [ATP] in the Dogic system results in a gelation transition from a fluid to a solid-like state<sup>22</sup> because kinesin motors act as long-lived passive linkers in the absence of ATP. Our second

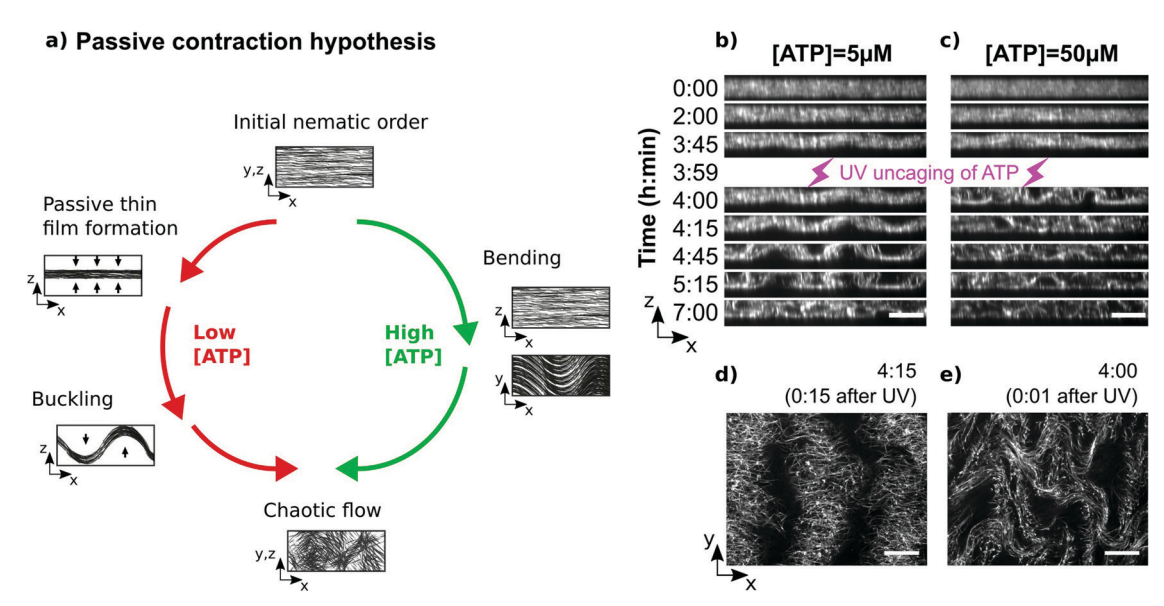


Fig. 4 The bending/buckling transition is not controlled by passive contraction. (a) Scheme of the kinetic hypothesis, where two instabilities are observed depending on ATP concentration. At low [ATP], activity is reduced, which lets the time for the passive contraction of microtubules to form a film that buckles. At high [ATP], the higher activity induces a bending instability. Confocal images of solutions with respectively 5 µM (b and d) and 50 µM (c and e) caged-ATP. Panels (b and c) provide time-lapses in the xz-plane with the uncaging event indicated at 3 h 59 min. Panels (d and e) display images in the xy-plane just after uncaging. Scale bars are 100  $\mu m$  in xy and 188  $\mu m$  in z. Pluronic 5.5% w/v.

hypothesis is thus that the gelation state of the active fluid determines the observed spatial instability, from in-plane bending in the fluid phase at high [ATP] to out-of-plane buckling in the solid phase at low [ATP] (Fig. 5a and b). In this subsection, we use a hydrodynamic active matter framework<sup>23–26</sup> to show that the observation of different instability modes is indeed consistent with a gelation transition controlled by crosslinking.

We model the kinesin-microtubule gel using a consistent description of an orientable and crosslinked active material described in ref. 27; this general theory is recapitulated in the ESI† and summarized here. We assume that at low [ATP] most kinesin motors act as passive crosslinkers, while at high [ATP] most motors are activated and therefore do not act as passive crosslinkers. The concentrations of passive or active motors do not appear directly in our theory; instead we start from a classical model of viscoelasticity228 where crosslinkers effectively control the relaxation rate  $1/\tau_C$  of a conformation tensor C, which characterizes the polymeric conformation of the microtubule filaments.  $\tau_C \rightarrow 0$  corresponds to a fluid state (at high [ATP]), while  $\tau_{\rm C} \to \infty$  corresponds to a solid state (at low [ATP]). In such a permanently crosslinked, solid regime, the deviation of the conformation tensor,  $\delta C$ , from its steady-state value is the classical strain tensor of the gel.27 Next, the degree of alignment of the microtubules is described by the nematic tensor Q, as is usual in the context of liquid crystals. Last, the dynamics of the gel is characterized by the fluid flow v. In the

main text, we display the equations of motion corresponding to the situation in which the gel fills the entire channel (which is the case at least at high [ATP]), for simplicity; we average the dynamics of the gel over the thickness of the channel and present the effective two-dimensional dynamics. These twodimensional hydrodynamic equations governing the dynamics of the coupled variables C, Q, v are

$$\partial_t \mathbf{Q} = \mathbf{Q} \cdot \omega - \omega \cdot \mathbf{Q} - 2\lambda \mathbf{A} + \frac{1}{\tau_O} \mathbf{H}$$
 (1)

$$\partial_t \mathbf{C} = \mathbf{C} \cdot \omega - \omega \cdot \mathbf{C} - 2\lambda_C \mathbf{A} + \frac{1}{\tau_C} \mathbf{B}$$
 (2)

$$\Gamma \mathbf{v} - \eta \nabla_{\perp}^{2} \mathbf{v} = -\nabla_{\perp} \Pi + \nabla_{\perp} \cdot \boldsymbol{\sigma}^{G}$$
 (3)

where  $\mathbf{A} = (1/2)[\nabla_{\perp}\mathbf{v} + (\nabla_{\perp}\mathbf{v})^T]$  and  $\omega = (1/2)[\nabla_{\perp}\mathbf{v} - (\nabla_{\perp}\mathbf{v})^T]$ .  $\mathbf{H} = -\delta F/\delta \mathbf{Q}$  and  $\mathbf{B} = -\delta F/\delta \mathbf{C}$  are the molecular fields corresponding to the nematic tensor and the conformation tensor respectively where F is the free energy that would control the dynamics in the absence of activity. Crucially, F includes a coupling between alignment Q and conformation C of the gel with a coefficient  $\chi$  (eqn (S8), ESI†), which is of the form  $2\chi C_{ij}Q_{ij}$ , where Einstein summation convention has been assumed for the indices. Further, Q and C are also coupled via their respective couplings to the fluid flow.  $\Pi$  enforces the

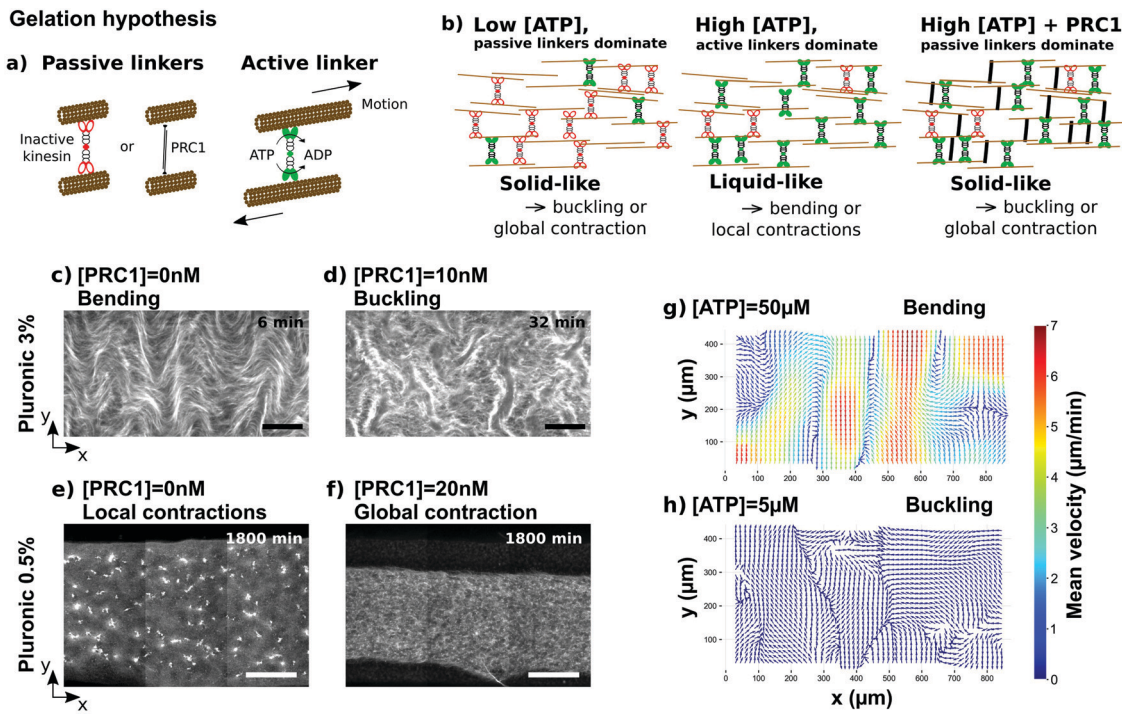


Fig. 5 The bending/buckling and local/global contraction transitions are controlled by the concentration of passive linkers that induce a gelation transition. (a) Schemes of passive linkers (ATP-depleted kinesin, in red, and PRC1 in black) and active one (ATP-consuming kinesin, in green). (b) Schemes of the active gel at different [ATP] and [PRC1] highlighting their liquid/solid-like state and the instabilities observed. Epifluorescence images showing the instabilities observed at high [ATP] (50 µM) and either high (c and d) or low (e and f) pluronic concentration and low (c and e) or high (d and f) [PRC1]. Scale bars are 200 µm for (c and d) and 500 µm for (e and f). (g and h) Particle image velocimetry of the bending (g) and buckling (h) instabilities observed at 0 nM PRC1, 5.5% pluronic and [ATP] as indicated. In panels (c-f) [MT] = 1 mg mL $^{-1}$ .

two-dimensional incompressibility constrain  $\nabla_{\perp} \cdot \mathbf{v} = 0$  and  $\sigma^G$  is the stress due to the gel which has the form described in ref. 27. Activity is introduced in the model via an active stress  $\zeta \mathbf{Q}$  – which we assume to depend only on the nematic order parameter – with  $\zeta > 0$  describing a system with an extensile uniaxial active stress. The remaining terms are required to ensure that the correct equilibrium physics is obtained in the absence of activity.

As we show in detail in the supplement, this formulation demonstrates that in the fluid limit ( $\tau_{\rm C} \to 0$ , associated to high [ATP]), and for high enough active drive  $\zeta$ , the classical in-plane bending instability characteristic of extensile fluids<sup>23,29,30</sup> is obtained (eqn (S24), ESI†). However, when  $\tau_{\rm C} \to \infty$  (associated with low [ATP]), *i.e.*, the gel is essentially solid, the bending instability is suppressed when  $\chi > 0$  (eqn (S63), ESI†). More quantitatively, in Fourier space, the stability of the gel to a pure bend perturbation with wavenumber  $q_{\perp}$  is determined by the negativity of the following eigenvalue:

$$\Xi = -\frac{q_{\perp}^{2}}{\tau_{Q} + 4\chi^{2}\tau_{C}} \left[ K - \frac{\tau_{Q}\zeta}{\Gamma} \left\{ 1 - \left( \lambda - \frac{2\lambda_{C}\chi\tau_{C}}{\tau_{Q}} \right) \right\} \right]$$
(4)

where K is the Frank elasticity of the nematic. Importantly, even when  $\zeta \gg K$  (*i.e.*, in the highly active regime), if  $\lambda_{\rm C} \to -1$  and  $\chi > 0$ , as we expect our system parameters to be, this eigenvalue goes from being destabilising (*i.e.*, positive) to stabilising (*i.e.*, negative) as  $\tau_{\rm C}$  is increased. This demonstrates that greater crosslinking, which leads to a gelation transition, stabilises the gel to bend perturbations.

This thickness averaged description cannot, however, account for the buckling transition since homogeneity along the z direction is assumed. In the supplement, we explicitly demonstrate that when this condition is relaxed and gel disposes of some space to deform in the z direction, it buckles out of plane because the extensile active stress  $\zeta \mathbf{Q}$  leads to a negative and destabilising surface tension along the uniaxial direction x, as previously shown<sup>5</sup> (eqn (S65), ESI†). In other words, a buckling gel does not bend in the high  $\tau_{\rm C}$  solid limit (at least initially). Finally, we also demonstrate that a gel in the fluid, low  $\tau_{\rm C}$  limit that may deform in the z direction, both bends and buckles (eqn (S71), ESI†).

To summarise, the four key results of the theoretical modelling are i. in-plane bend instability at low  $\tau_{\rm C}$  (fluid limit), ii. suppression of this instability at high  $\tau_{\rm C}$  (solid limit), iii. buckling instability in the high  $\tau_{\rm C}$  solid limit, when the gel does not homogeneously fill the channel and iv. both buckling and bending instability in the low  $\tau_{\rm C}$  fluid limit when the gel can deform in the z direction. These theoretical results are compatible with the previous experimental observations if we assume, based on Gagnon  $et\ al.$ ,  $^{22}$  that [ATP] drives a gelation transition in the Dogic system. In particular, the third and fourth theoretical results are consistent with buckling being observed at low [ATP] and a mixture of buckling and bending at high [ATP] when the active system may deform in the z axis, as shown in the experiments in Fig. 4.

Note that while we assumed that passive motors act as crosslinkers, the theory is insensitive to the chemical nature of crosslinkers. This suggests that adding passive crosslinkers in a gel, while keeping high ATP and pluronic concentrations, should modify the instability mode of the gel.

Our linear stability theory applies to buckling/bending instabilities that arise close to the initial nematic state but does not inform us about global/local contraction instabilities that happen far from this state. However, the global/local contraction transition has been demonstrated to be associated to a gelation transition in actin gels.  $^{10}$  These results, together with Gagnon's *et al.* and Fig. 3 suggest that both the bending/buckling and the global/local contraction transitions at  $\sim$  10  $\mu$ M ATP are due to a gelation transition.

# 2.3 The bending/buckling and local/global contraction transitions are controlled by the concentration of passive linkers

To experimentally challenge the gelation hypothesis, we introduced passive PRC1 linkers<sup>4</sup> at constant [ATP]. At high pluronic, we observed that 10 nM PRC1 was sufficient to convert a bending into a buckling instability (Fig. 5c, d and Movie S7, ESI†). At low pluronic, a system displaying local contractions in the absence of PRC1 displayed global ones at 20 nM PRC1 (Fig. 5e, f and Movie S8, ESI†). In some occasions, we observed that a bending state became global contraction when PRC1 was added (Fig. S6, ESI†). Importantly, the characteristic times of the bending/buckling instabilities, on the one hand, and of the local/global contraction instabilities, on the other hand, were similar at constant [ATP] and different PRC1 (Table S4, ESI†), in agreement with experiments at [ATP]c (Fig. S3, ESI†) and in contrast with what was observed at different [ATP] in the absence of PRC1 (Table S3, ESI†).

The gelation transition occurred at [ATP]<sub>c</sub>  $\approx 10~\mu M$  in Fig. 3. Using a Michaelis–Menten model, we can estimate the concentration of passive motors as  $c_{\rm m}^{\rm p} = c_{\rm m}^{\rm 0}~(1-[{\rm ATP}]/(K_M+[{\rm ATP}]))$ , where  $c_{\rm m}^{\rm 0}$  is the concentration of all motors and  $K_M=40$ –60  $\mu M$  is the Michaelis–Menten constant of kinesin-1 motor and ATP. Taking  $c_{\rm m}^{\rm 0}=25~{\rm nM}$  for our experiments, one finds  $c_{\rm m}^{\rm p}\approx 20~{\rm nM}$ , which corresponds to a concentration of passive linkers  $c_{\rm m}^{\rm p}\approx 5~{\rm nM}$  (Fig. S7, ESI†). This result is consistent with the gelation transition observed at 10 and 20 nM PRC1, respectively for bending/buckling and local/global contractions (Fig. 5c-f).

To further test the gelation hypothesis, we quantified the average velocity flows of the microtubules in the *xy*-plane during the bending and buckling instabilities at different [ATP] in the absence of PRC1 (Fig. 5g and h). During bending, strong flows up to  $7 \mu \text{m min}^{-1}$  arise parallel to the *y* axis as observed previously.<sup>4,14</sup> In contrast, during buckling the flows do not show a clear structure and they are significantly smaller, on the order of 0.4  $\mu \text{m min}^{-1}$ , as expected for a solid. The correlation along *x* of the velocity orientation angles confirms this interpretation (Fig. S8, ESI†).

These observations clearly show that a large fraction of kinesin motors act as passive crosslinkers at low [ATP] but not at high [ATP], implying that [ATP] controls a transition from

a crosslinked gel to a fluid that determines the spatial instability displayed by the active gel.

### 3 Conclusion

We have observed four important spatial instabilities - bending, buckling, local and global contractions - in a single type of cytoskeletal active gel and we have shown that they are determined by two factors: the crosslinking of the gel and the concentration of depletion agent. Our theoretical and experimental results demonstrate that the bending-to-buckling and local-toglobal contraction transitions are determined by a gelation transition in the active gel, induced either by motors acting as passive crosslinkers when [ATP] decreases, or by passive linkers at a fixed [ATP]. However, although the depletant concentration is known to promote filament bundling,<sup>33</sup> it is not yet clear how this property controls the bending-to-local contraction and buckling-to-global contraction transitions.

Our work generalizes previous results that showed that the local-to-global contraction transition is controlled by the percolation of the gel induced by passive linkers in actin-myosin gels.10 Building on previous work,22 our results underline the dual role of motors both as passive and active linkers in cytoskeletal active gels. In particular, we show, by varying [ATP], that motors not only control the degree of active drive, as is generally assumed in active fluid theories,5,14 but also the mechanical properties of the gel, leading to qualitatively distinct spatial instabilities and gel morphologies. In summary, this work provides a unified view of spatial instabilities in cytoskeletal active gels and provides an experimental and theoretical framework to design active materials with controllable out-of-equilibrium properties. 19,34-36

#### 4 Materials and methods

#### **Active solution**

Active linkers are clusters of streptavidin and biotinylated kinesin-1. The active solution was composed of fluorescent GMPCPP-stabilized microtubules (at 0.5-1 mg mL<sup>-1</sup>), kinesin and streptavidin (both at a concentration of 25 nM), ATP and pluronic (from 1 µM to 100 µM and from 1.5% to 5.5%, respectively), an ionic buffer, an antioxydant mix and an ATP regeneration system.

#### **Imaging**

The active solution was injected into rectangular cross-section channels (22  $\times$  1.5  $\times$  0.13 mm) made using passivated glass slides separated by parafilm. Imaging was done by epifluorescence or confocal microscopy at room temperature.

#### **Analysis**

Images were reconstructed with Fiji and analyzed with Python scripts, using openpiv package for PIV analysis.

See Supporting Information for a more detailed description.

#### Conflicts of interest

There are no conflicts to declare.

## Acknowledgements

Z. Gueroui for a kind gift of the K401 plasmid, F. Lam from the microscopy platform at IBPS, L. L. Pontani for providing access to a spinning disk microscope, and A. Senoussi, Y. Vyborna and G. Duclos for insightful discussions. This work has been funded by the European Research Council (ERC) under the European's Union Horizon 2020 programme (grant No 770940, A. E.-T.). A. M. was supported by a TALENT fellowship from CY Cergy Paris Université. For PRC1 synthesis, we acknowledge support from Brandeis NSF MRSEC, Bioinspired Soft Materials, DMR-2011846. In the concluding stages of our work, we became aware of a complementary, independent effort by the group of Guillaume Duclos who studied instabilities in kinesinmicrotubule active fluids.37

### References

- 1 M. C. Marchetti, J.-F. Joanny, S. Ramaswamy, T. B. Liverpool, J. Prost, M. Rao and R. A. Simha, Hydrodynamics of soft active matter, Rev. Mod. Phys., 2013, 85, 1143.
- 2 D. Needleman and Z. Dogic, Active matter at the interface between materials science and cell biology, Nat. Rev. Mater., 2017, 2, 17048.
- 3 A. Bricard, J.-B. Caussin, N. Desreumaux, O. Dauchot and D. Bartolo, Emergence of macroscopic directed motion in populations of motile colloids, *Nature*, 2013, **503**, 95.
- 4 P. Chandrakar, M. Varghese, S. Aghvami, A. Baskaran, Z. Dogic and G. Duclos, Confinement Controls the Bend Instability of Three-Dimensional Active Liquid Crystals, Phys. Rev. Lett., 2020, 125, 257801.
- 5 A. Senoussi, S. Kashida, R. Voituriez, J.-C. Galas, A. Maitra and A. Estevez-Torres, Tunable corrugated patterns in an active nematic sheet, Proc. Natl. Acad. Sci. U. S. A., 2019, 116, 22464-22470.
- 6 T. Strübing, A. Khosravanizadeh, A. Vilfan, E. Bodenschatz, R. Golestanian and I. Guido, Wrinkling Instability in 3D Active Nematics, Nano Lett., 2020, 6281-6288.
- 7 Y. Ideses, V. Erukhimovitch, R. Brand, D. Jourdain, J. S. Hernandez, U. Gabinet, S. Safran, K. Kruse and A. Bernheim-Groswasser, Spontaneous buckling of contractile poroelastic actomyosin sheets, Nat. Commun., 2018, 9, 2461.
- 8 P. M. Bendix, G. H. Koenderink, D. Cuvelier, Z. Dogic, B. N. Koeleman, W. M. Brieher, C. M. Field, L. Mahadevan and D. A. Weitz, A quantitative analysis of contractility in active cytoskeletal protein networks, Biophys. J., 2008, 94, 3126-3136.
- 9 T. Torisawa, D. Taniguchi, S. Ishihara and K. Oiwa, Spontaneous Formation of a Globally Connected Contractile Network in a Microtubule-Motor System, Biophys. J., 2016, 111, 373-385.

Published on 27 April 2022. Downloaded on 3/31/2023 7:41:27 PM

Paper

10 J. Alvarado, M. Sheinman, A. Sharma, F. C. MacKintosh and

- G. H. Koenderink, Molecular motors robustly drive active gels to a critically connected state, Nat. Phys., 2013, 9, 591-597.
- 11 P. J. Foster, S. Fuerthauer, M. J. Shelley and D. J. Needleman, Active contraction of microtubule networks, eLife, 2015, 4, e10837.
- 12 F. J. Nédélec, T. Surrey, A. C. Maggs and S. Leibler, Selforganization of microtubules and motors, Nature, 1997, 389, 305-308.
- 13 T. Sanchez, D. T. N. Chen, S. J. DeCamp, M. Heymann and Z. Dogic, Spontaneous motion in hierarchically assembled active matter, Nature, 2012, 491, 431-434.
- 14 B. Martnez-Prat, J. Ignés-Mullol, J. Casademunt and F. Sagués, Selection mechanism at the onset of active turbulence, Nat. Phys., 2019, 15, 362.
- 15 N. Kumar, R. Zhang, J. J. de Pablo and M. L. Gardel, Tunable structure and dynamics of active liquid crystals, Sci. Adv., 2018, 4, eaat7779.
- 16 T. Surrey, F. Nedelec, S. Leibler and E. Karsenti, Physical properties determining self-organization of motors and microtubules, Science, 2001, 292, 1167-1171.
- 17 V. Nasirimarekani, T. Strübing, A. Vilfan and I. Guido, Tuning the Properties of Active Microtubule Networks by Depletion Forces, Langmuir, 2021, 37, 7919-7927.
- 18 A. Senoussi, J.-C. Galas and A. Estevez-Torres, Programmed mechano-chemical coupling in reaction-diffusion active matter, bioRxiv, 2021, DOI: 10.1101/2021.03.13.435232.
- 19 A. Senoussi, J.-C. Galas and A. Estevez-Torres, Programmed mechano-chemical coupling in reaction-diffusion active matter, Sci. Adv., 2021, 7, eabi9865.
- 20 B. Lemma, N. P. Mitchell, R. Subramanian, D. J. Needleman and Z. Dogic, Active microphase separation in mixtures of microtubules and tip-accumulating molecular motors. arXiv:2107.12281 [cond-mat, physics:physics], 2021.
- 21 J. Roostalu, J. Rickman, C. Thomas, F. Nedelec and T. Surrey, Determinants of Polar versus Nematic Organization in Networks of Dynamic Microtubules and Mitotic Motors, Cell, 2018, 175, 796-808.
- 22 D. A. Gagnon, C. Dessi, J. P. Berezney, R. Boros, D. T.-N. Chen, Z. Dogic and D. L. Blair, Shear-Induced Gelation of Self-Yielding Active Networks, Phys. Rev. Lett., 2020, 125, 178003.
- 23 M. C. Marchetti, J. F. Joanny, S. Ramaswamy, T. B. Liverpool, J. Prost, M. Rao and R. A. Simha, Hydrodynamics of soft active matter, Rev. Mod. Phys., 2013, 85, 1143-1189.

- 24 S. Ramaswamy, The Mechanics and Statistics of Active Matter, Annu. Rev. Condens. Matter Phys., 2010, 1, 323-345.
- 25 J. Prost, F. Jülicher and J.-F. Joanny, Active gel physics, Nat. Phys., 2015, 11, 111-117.
- 26 F. Jülicher, S. W. Grill and G. Salbreux, Hydrodynamic theory of active matter, Rep. Prog. Phys., 2018, 81, 076601.
- 27 E. J. Hemingway, A. Maitra, S. Banerjee, M. C. Marchetti, S. Ramaswamy, S. M. Fielding and M. E. Cates, Active Viscoelastic Matter: From Bacterial Drag Reduction to Turbulent Solids, Phys. Rev. Lett., 2015, 114, 098302.
- 28 A. N. Beris and B. J. Edwards, Thermodynamics of Flowing Systems: with Internal Microstructure, Oxford Engineering Science Series Oxford University Press, New York, 1994, p. 704.
- 29 R. Voituriez, J. F. Joanny and J. Prost, Spontaneous flow transition in active polar gels, Europhys. Lett., 2005, 70, 404-410.
- 30 R. Aditi Simha and S. Ramaswamy, Hydrodynamic Fluctuations and Instabilities in Ordered Suspensions of Self-Propelled Particles, Phys. Rev. Lett., 2002, 89, 058101.
- 31 M. J. Schnitzer and S. M. Block, Kinesin hydrolyses one ATP per 8-nm step, Nature, 1997, 388, 386-390.
- 32 W. Hua, E. C. Young, M. L. Fleming and J. Gelles, Coupling of kinesin steps to ATP hydrolysis, Nature, 1997, 388, 390-393.
- 33 D. J. Needleman, M. A. Ojeda-Lopez, U. Raviv, K. Ewert, J. B. Jones, H. P. Miller, L. Wilson and C. R. Safinya, Synchrotron X-ray Diffraction Study of Microtubules Buckling and Bundling under Osmotic Stress: A Probe of Interprotofilament Interactions, Phys. Rev. Lett., 2004, 93, 198104.
- 34 Y. Vyborna, J.-C. Galas and A. Estevez-Torres, DNA-Controlled Spatiotemporal Patterning of a Cytoskeletal Active Gel, J. Am. Chem. Soc., 2021, 143, 20022-20026.
- 35 T. D. Ross, H. J. Lee, Z. Qu, R. A. Banks, R. Phillips and M. Thomson, Controlling Organization and Forces in Active Matter Through Optically-Defined Boundaries, Nature, 2019, 572, 224-229, arXiv: 1812.09418.
- 36 A. M. Tayar, M. F. Hagan and Z. Dogic, Active liquid crystals powered by force-sensing DNA-motor clusters, Proc. Natl. Acad. Sci. U. S. A., 2021, 118, e2102873118.
- 37 B. Najma, M. Varghese, L. Tsidilkovski, L. Lemma, A. Baskaran and G. Duclos, Dual antagonistic role of motor proteins in fluidizing active networks. arXiv:2112.11364 [cond-mat, physics:physics], 2021.